CHAPTER

Field Problems: A Multidimensional Finite Element Method

5

5.1 Field problems: Quasi-harmonic equation

The general procedures discussed in the previous two chapters can be applied to a variety of physical problems. Here we shall deal with situations governed by the general "quasi-harmonic" equation described in Chapter 2 and solved by finite element methods in Chapters 3 and 4 for the one-dimensional case. Particular cases of the equation are the well-known Laplace, Poisson, and Helmholtz equations [1–6]. The range of physical problems falling into this category is large. To list but a few frequently encountered in engineering practice we have:

- Heat conduction
- Seepage through porous media
- Irrotational flow of ideal fluids
- Distribution of electrical (or magnetic) potential
- Torsion of prismatic shafts
- Lubrication of pad bearings, etc.

The formulation developed in this chapter is equally applicable to all, and hence only limited reference will be made to the actual physical quantities. In all the above classes of problems, the behavior can be represented in terms of a scalar variable for which we will generally use the symbol ϕ as the physical variable describing the behavior. However, in discussing heat conduction applications ϕ becomes the temperature which we will denote by the symbol T. Similar changes will be made when discussing other specific physical problems.

In general Cartesian coordinates we recall that the balance equation for the flux $\mathbf{q}$ is given by [viz. (2.78)]

$$-\left(\frac{\partial q_x}{\partial x}+\frac{\partial q_y}{\partial y}+\frac{\partial q_z}{\partial z}\right)+Q=c\frac{\partial \phi}{\partial t} \tag{5.1}$$

Following the steps described in (3.1) a weak form for the equation may be written as

$$\mathrm{G}(\delta\phi,\phi,\mathbf{q})=\int_\Omega \delta\phi\left[c\frac{\partial \phi}{\partial t}+\left(\frac{\partial q_x}{\partial x}+\frac{\partial q_y}{\partial y}+\frac{\partial q_z}{\partial z}\right)-Q\right]\mathrm{d}\Omega=0 \tag{5.2}$$

The Finite Element Method: Its Basis and Fundamentals. http://dx.doi.org/10.1016/B978-1-85617-633-0.00005-8

After integration by parts the weak form becomes

$$\begin{aligned} \mathrm{G}(\delta\phi, \phi, \mathbf{q}) = &\int_\Omega \delta\phi \left[c\frac{\partial \phi}{\partial t} - Q \right] \mathrm{d}\Omega + \int_{\Gamma_q} \delta\phi\, \bar{q}_n \,\mathrm{d}\Gamma \\ &- \int_\Omega \begin{bmatrix} \dfrac{\partial \delta\phi}{\partial x} & \dfrac{\partial \delta\phi}{\partial y} & \dfrac{\partial \delta\phi}{\partial z} \end{bmatrix} \begin{Bmatrix} q_x \\ q_y \\ q_z \end{Bmatrix} \mathrm{d}\Omega = 0 \end{aligned} \tag{5.3}$$

where $q_n = \mathbf{n}^{\mathrm{T}}\mathbf{q}$ is the flux normal to the boundary with $\mathbf{n}$ the outward pointing boundary normal. In the above we have also split the boundary term as

$$\int_\Gamma \delta\phi\, q_n \,\mathrm{d}\Gamma = \int_{\Gamma_\phi} \delta\phi\, q_n \,\mathrm{d}\Gamma + \int_{\Gamma_q} \delta\phi\, \bar{q}_n \,\mathrm{d}\Gamma \tag{5.4}$$

and assumed $\phi = \bar{\phi}$ is satisfied such that we may set $\delta\phi = 0$ on Γ_ϕ. We also recall from Section 2.3.2 that $\bar{q}_n$ can include boundary radiation effects as

$$\bar{q}_n = \bar{q} + H(\phi - \phi_0)$$

which we will use in some of the subsequent developments.

5.1.1 Irreducible form

To obtain an irreducible form we introduce a linear relationship to relate the flux to the gradient of ϕ. The form was given in (2.83) as

$$\mathbf{q} = -\mathbf{k}\,\nabla\phi \tag{5.5}$$

where $\mathbf{k}$ is a symmetric matrix of coefficients and

$$\nabla\phi = \begin{Bmatrix} \dfrac{\partial \phi}{\partial x} \\ \dfrac{\partial \phi}{\partial y} \\ \dfrac{\partial \phi}{\partial z} \end{Bmatrix} \tag{5.6}$$

denotes the *gradient* of ϕ. We also recall that the relationship is known as Fourier's, Fick's, or Darcy's law depending on which physical problem we consider.

Introducing (5.5) into (5.3) for a general three-dimensional problem yields the desired irreducible form

$$\begin{aligned} \mathrm{G}(\delta\phi, \phi) = &\int_\Omega \delta\phi \left[c\frac{\partial \phi}{\partial t} - Q \right] \mathrm{d}\Omega + \int_\Omega (\nabla\delta\phi)^{\mathrm{T}}\mathbf{k}\,\nabla\phi \,\mathrm{d}\Omega \\ &+ \int_{\Gamma_q} \delta\phi \left[\bar{q} + H(\phi - \phi_0) \right] \mathrm{d}\Gamma = 0 \end{aligned} \tag{5.7}$$

5.1.2 Finite element discretization

The finite element solution process follows the standard solution methodology introduced in Chapter 3. For the quasi-harmonic equation approximates the trial function using C_0 shape functions we use

$$\phi \approx \hat{\phi} = \sum_a N_a \tilde{\phi}_a = \mathbf{N}\tilde{\boldsymbol{\phi}} \tag{5.8}$$

in the weak formulation (5.7) together a similar expression for $\delta\phi$.

We define the approximation to the gradient of ϕ as

$$\begin{aligned} \nabla\hat{\phi} &= \sum_a (\nabla N_a)\tilde{\phi}_a \\ &= \sum_a \begin{bmatrix} \dfrac{\partial N_a}{\partial x} & \dfrac{\partial N_a}{\partial y} & \dfrac{\partial N_a}{\partial z} \end{bmatrix}^{\mathrm{T}} \tilde{\phi}_a = \sum_a \mathbf{b}_a \tilde{\phi}_a \end{aligned} \tag{5.9}$$

where $\mathbf{b}_a$ denotes the *gradient matrix*.

5.1.2.1 Two-dimensional plane and axisymmetric problem

The two-dimensional *plane case* is obtained by taking the gradient in the form

$$\nabla = \begin{bmatrix} \dfrac{\partial}{\partial x} & \dfrac{\partial}{\partial y} \end{bmatrix}^{\mathrm{T}} \tag{5.10}$$

and taking the flux as

$$\mathbf{q} = \begin{Bmatrix} q_x \\ q_y \end{Bmatrix} = -\begin{bmatrix} k_{xx} & k_{xy} \\ k_{yx} & k_{yy} \end{bmatrix} \begin{Bmatrix} \dfrac{\partial \phi}{\partial x} \\ \dfrac{\partial \phi}{\partial y} \end{Bmatrix} \tag{5.11}$$

On discretization a slightly simplified form of the matrices will now be found with $\mathbf{b}_a$ in Eq. (5.9) replaced by

$$\mathbf{b}_a = \begin{bmatrix} \dfrac{\partial N_a}{\partial x} & \dfrac{\partial N_a}{\partial y} \end{bmatrix}^{\mathrm{T}} \tag{5.12}$$

and the volume element replaced by

$$\mathrm{d}\Omega = h_z \,\mathrm{d}x\,\mathrm{d}y$$

where h_z is the slab thickness. Alternatively the formulation may be specialized to cylindrical coordinates and used for the solution of *axisymmetric* situations by introducing the gradient

$$\nabla = \begin{bmatrix} \dfrac{\partial}{\partial r} & \dfrac{\partial}{\partial z} \end{bmatrix}^{\mathrm{T}} \tag{5.13}$$

where r, z replace x, y to describe both the gradient and $\mathbf{b}_a$. With the flux now given by

$$\mathbf{q} = \begin{Bmatrix} q_r \\ q_z \end{Bmatrix} = -\begin{bmatrix} k_{rr} & k_{rz} \\ k_{zr} & k_{zz} \end{bmatrix} \begin{Bmatrix} \dfrac{\partial \phi}{\partial r} \\ \dfrac{\partial \phi}{\partial z} \end{Bmatrix} \tag{5.14}$$

the discretization is now performed with the volume element expressed by

$$\mathrm{d}\Omega = 2\pi r \, \mathrm{d}r \, \mathrm{d}z$$

5.1.2.2 *Element matrices*

Substituting (5.8) and (5.9) into (5.7), we obtain a typical element contribution as

$$\widehat{\mathrm{G}}_e(\delta\hat{\phi}, \hat{\phi}) = \delta\tilde{\phi}_a \left[C^e_{ab}\dot{\tilde{\phi}}_b + H^e_{ab}\tilde{\phi}_b - s^e_a \right] \tag{5.15}$$

where

$$\begin{aligned} C^e_{ab} &= \int_{\Omega_e} N_a c N_b \, \mathrm{d}\Omega \\ H^e_{ab} &= \int_{\Omega_e} \mathbf{b}_a^{\mathrm{T}} \mathbf{k} \mathbf{b}_b \, \mathrm{d}\Omega + \int_{\Gamma_{qe}} N_a H N_b \, \mathrm{d}\Gamma \\ s^e_a &= \int_{\Omega_e} N_a Q \, \mathrm{d}\Omega - \int_{\Gamma_{qe}} N_a(\bar{q} - H\phi_0)\mathrm{d}\Gamma \end{aligned} \tag{5.16}$$

define the matrix contributions to each element.

Evaluating the integrals and assembling all elements leads to the set of standard semi-discrete equations of the form

$$\mathbf{C}\dot{\tilde{\boldsymbol{\phi}}} + \mathbf{H}\tilde{\boldsymbol{\phi}} = \mathbf{s} \tag{5.17}$$

to which prescribed values of $\bar{\phi}$ have to be imposed on boundaries Γ_ϕ. We again note that an additional "stiffness" is contributed on any boundaries for which a radiation constant H is specified. Solution of the semi-discrete equations is considered in the next section. However, for steady-state problems the first term may be ignored and the problem solved to give

$$\tilde{\boldsymbol{\phi}} = \mathbf{H}^{-1}\mathbf{s}$$

After solution the same standard operations are followed to evaluate the fluxes using

$$\mathbf{q} \equiv -\mathbf{k}\,\nabla\phi = -\mathbf{k}\sum_a \mathbf{b}_a \tilde{\phi}_a \tag{5.18}$$

The fluxes may be easily computed within the elements; however, it is often desirable to obtain their values at nodes. This is best accomplished by the procedure to be described in Section 7.8. However, here we summarize a simple averaging method.

A least squares method may be used to project the element flux to nodal values using a functional

$$\Pi_q = \frac{1}{2}\sum_e \int_{\Omega_e} \left(q^\star - \hat{q}(\mathbf{x})\right)^2 \mathrm{d}\Omega = \text{minimum}$$

where q is any component of the flux, $\hat{q}$ is the element flux, and $q^\star$ is given in each element by

$$q^\star = \sum_a N_a \tilde{q} = \mathbf{N}\tilde{\mathbf{q}}$$

Minimizing the functional gives

$$\mathbf{M}\tilde{\mathbf{q}} = \sum_e \int_{\Omega_e} \mathbf{N}^{\mathrm{T}} \hat{q}(\mathbf{x}) \mathrm{d}\Omega = \mathbf{f}$$

where

$$\mathbf{M} = \sum_e \int_{\Omega_e} \mathbf{N}^{\mathrm{T}}\mathbf{N}\,\mathrm{d}\Omega$$

The solution becomes trivial if we *diagonalize* $\mathbf{M}$ (see Appendix H) since then we obtain

$$\tilde{\mathbf{q}} = \mathbf{M}^{-1}\mathbf{f}$$

by simple divisions. An alternative to the above is the use of a local least squares on each individual element followed by averaging at each node [7].

5.1.3 Shape functions for triangle, rectangle, and tetrahedron

To compute the element matrices given in (5.16) it is necessary to devise appropriate shape functions. Here for two-dimensional problems we consider the simplest form for elements of triangular and rectangular form. For three-dimensional problems the simple tetrahedral element form is also developed. In the next chapter we generalize these to create families of elements for use in all problems for which C_0 approximations are needed.

5.1.3.1 Triangle with three nodes

The finite element domain is defined by dividing Ω into a mesh of two-dimensional triangular elements as shown in Fig. 5.1a. A simple set of C_0 functions can be constructed from linear polynomials over three-node triangles as shown in Fig. 5.1b. This element was first used to solve a variational equilibrium problem by Courant [8]. Later Turner et al. used the element to solve plane elasticity problems [9].

The approximation in each triangle may be written as a linear function of the Cartesian coordinates

$$\hat{\phi}^e = \alpha_1 + \alpha_2 x + \alpha_3 y$$

The parameters α_1 to α_3 may be evaluated in terms of the displacements at each of the three vertices of the triangle. The vertices define the nodes of the triangle.

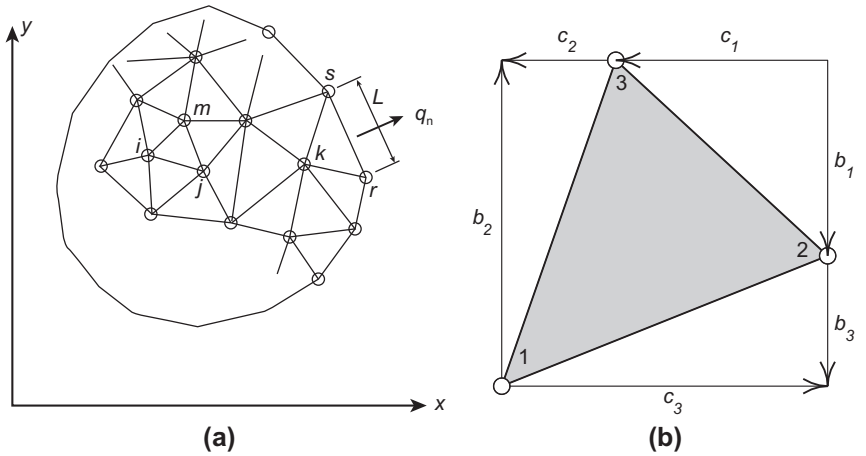

FIGURE 5.1
Division of a two-dimensional region into triangular elements: (a) triangular mesh and (b) geometry of triangle.

Accordingly, we write the set of equations

$$\begin{Bmatrix} \tilde{\phi}_1^e \\ \tilde{\phi}_2^e \\ \tilde{\phi}_3^e \end{Bmatrix} = \begin{bmatrix} 1 & x_1 & y_1 \\ 1 & x_2 & y_2 \\ 1 & x_3 & y_3 \end{bmatrix} \begin{Bmatrix} \alpha_1 \\ \alpha_2 \\ \alpha_3 \end{Bmatrix}$$

where x_a and y_a are coordinates at the three vertices of the triangle. The inverse to the coefficient matrix is given by

$$\begin{bmatrix} 1 & x_1 & y_1 \\ 1 & x_2 & y_2 \\ 1 & x_3 & y_3 \end{bmatrix}^{-1} = \frac{1}{2\Delta} \begin{bmatrix} a_1 & a_2 & a_3 \\ b_1 & b_2 & b_3 \\ c_1 & c_2 & c_3 \end{bmatrix}$$

where

$$\begin{aligned} a_1 &= x_2y_3 - x_3y_2, & b_1 &= y_2 - y_3, & c_1 &= x_3 - x_2 \\ a_2 &= x_3y_1 - x_1y_3, & b_2 &= y_3 - y_1, & c_2 &= x_1 - x_3 \\ a_3 &= x_1y_2 - x_2y_1, & b_3 &= y_1 - y_2, & c_3 &= x_2 - x_1 \end{aligned}$$

and $\Delta = (x_1b_1 + x_2b_2 + x_3b_3)/2$ is the area of the triangle. The meaning of the b_a and c_a parameters is shown in Fig. 5.1b.

The above solution for the parameters α_a permits the element interpolations to be rewritten in terms of nodal parameters as

$$\hat{\phi}^e = \sum_{a=1}^{3} \frac{1}{2\Delta} \left(a_a + b_a x + c_a y\right) \tilde{\phi}_a^e$$

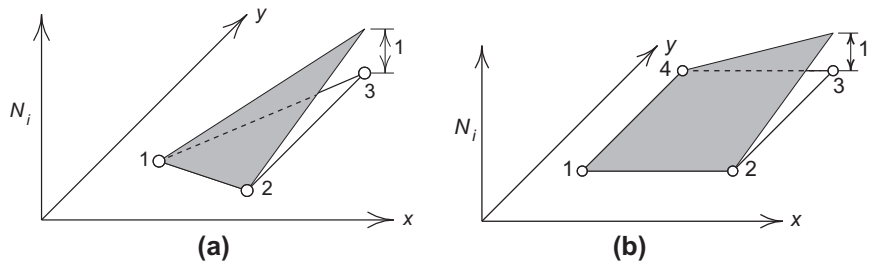

FIGURE 5.2
Shape function N_3 for one element: (a) three-node triangle and (b) four-node rectangle.

Thus, the three shape functions for the triangle are given by

$$N_a(x, y) = \frac{1}{2\Delta}\left(a_a + b_a x + c_a y\right), \quad a = 1, 2, 3 \tag{5.19}$$

The shape function for $a = 3$ is shown in Fig. 5.2a. With this definition it is clear that we can write the set of approximations in each individual element as

$$\hat{\phi}^e = \sum_{a=1}^{3} N_a(x, y)\tilde{\phi}_a^e$$

Since these shape functions vary linearly along any side of a triangle, with identical nodal values imposed, the same value of the function will clearly exist along an interface between adjacent elements. We note, however, that the derivatives may not be continuous between elements; consequently, the above form only provides C_0 continuity.

5.1.3.2 *Rectangle with four nodes*

As a second example of two-dimensional shape functions we consider rectangles of the form shown in Fig. 5.3. The rectangular element considered has side lengths of $2a$ and $2b$ in the x- and y-directions, respectively. For the derivation of the shape functions it is convenient to use a local Cartesian system x', y' defined by

$$x' = x - x_0 \quad \text{and} \quad y' = y - y_0$$

where

$$x_0 = \frac{1}{4}\sum_{a=1}^{4} y_a \quad \text{and} \quad y_0 = \frac{1}{4}\sum_{a=1}^{4} x_a$$

in which x_0, y_0 are located at the center of the rectangle and x_a, y_a are coordinates of the nodes. We now need four functions for each displacement component in order to uniquely define the shape functions. In addition these functions must have linear

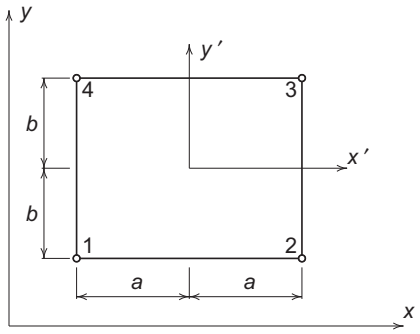

FIGURE 5.3
Rectangular element geometry and local node numbers.

behavior along each edge of the element to ensure interelement C_0 continuity. A suitable choice is given by

$$\hat{\phi}^e = \alpha_1 + x'\alpha_2 + y'\alpha_3 + x'y'\alpha_4 \tag{5.20}$$

The coefficients α_a may be obtained by expressing (5.20) at each vertex node giving

$$\begin{Bmatrix} \tilde{\phi}_1^e \\ \tilde{\phi}_2^e \\ \tilde{\phi}_3^e \\ \tilde{\phi}_4^e \end{Bmatrix} = \begin{bmatrix} 1 & -a & -b & ab \\ 1 & a & -b & -ab \\ 1 & a & b & ab \\ 1 & -a & b & -ab \end{bmatrix} \begin{Bmatrix} \alpha_1 \\ \alpha_2 \\ \alpha_3 \\ \alpha_4 \end{Bmatrix}$$

We can again solve for α_a in terms of the nodal displacements to obtain finally

$$\begin{aligned} \hat{\phi}^e = {} & \frac{1}{4}\left(1 - \frac{x'}{a}\right)\left(1 - \frac{y'}{b}\right)\tilde{\phi}_1^e + \frac{1}{4}\left(1 + \frac{x'}{a}\right)\left(1 - \frac{y'}{b}\right)\tilde{\phi}_2^e \\ & + \frac{1}{4}\left(1 + \frac{x'}{a}\right)\left(1 + \frac{y'}{b}\right)\tilde{\phi}_3^e + \frac{1}{4}\left(1 - \frac{x'}{a}\right)\left(1 + \frac{y'}{b}\right)\tilde{\phi}_4^e \end{aligned} \tag{5.21}$$

From (5.21) we obtain the four shape functions

$$\begin{aligned} N_1 &= \frac{1}{4}\left(1 - \frac{x'}{a}\right)\left(1 - \frac{y'}{b}\right), & N_2 &= \frac{1}{4}\left(1 + \frac{x'}{a}\right)\left(1 - \frac{y'}{b}\right) \\ N_3 &= \frac{1}{4}\left(1 + \frac{x'}{a}\right)\left(1 + \frac{y'}{b}\right), & N_4 &= \frac{1}{4}\left(1 - \frac{x'}{a}\right)\left(1 + \frac{y'}{b}\right) \end{aligned} \tag{5.22}$$

The shape function for N_3 is shown in Fig. 5.2b.

5.1.3.3 *Tetrahedron with four nodes*

For three-dimensional problems a simple element is a tetrahedron with four nodes as shown in Fig. 5.4. A C_0 compatible displacement field is again given

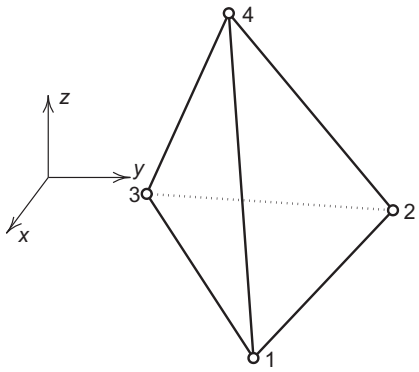

FIGURE 5.4
Tetrahedron element.

by a complete linear polynomial expansion as

$$\hat{\phi}^e = [\,1 \quad x \quad y \quad z\,] \begin{Bmatrix} \alpha_1 \\ \alpha_2 \\ \alpha_3 \\ \alpha_4 \end{Bmatrix} \tag{5.23}$$

The parameters α_a can be evaluated by evaluating (5.23) at each of the vertex nodes of the tetrahedron. Accordingly we have

$$\begin{Bmatrix} \tilde{\phi}_1^e \\ \tilde{\phi}_2^e \\ \tilde{\phi}_3^e \\ \tilde{\phi}_4^e \end{Bmatrix} = \begin{bmatrix} 1 & x_1 & y_1 & z_1 \\ 1 & x_2 & y_2 & z_2 \\ 1 & x_3 & y_3 & z_3 \\ 1 & x_4 & y_4 & z_4 \end{bmatrix} \begin{Bmatrix} \alpha_1 \\ \alpha_2 \\ \alpha_3 \\ \alpha_4 \end{Bmatrix}$$

The inverse is expressed as

$$\begin{bmatrix} 1 & x_1 & y_1 & z_1 \\ 1 & x_2 & y_2 & z_2 \\ 1 & x_3 & y_3 & z_3 \\ 1 & x_4 & y_4 & z_4 \end{bmatrix}^{-1} = \frac{1}{6V} \begin{bmatrix} a_1 & a_2 & a_3 & a_4 \\ b_1 & b_2 & b_3 & b_4 \\ c_1 & c_2 & c_3 & c_4 \\ d_1 & d_2 & d_3 & d_4 \end{bmatrix}$$

where

$$6V = \det \begin{bmatrix} 1 & x_1 & y_1 & z_1 \\ 1 & x_2 & y_2 & z_2 \\ 1 & x_3 & y_3 & z_3 \\ 1 & x_4 & y_4 & z_4 \end{bmatrix} \tag{5.24a}$$

and

$$a_1 = \det\begin{bmatrix} x_2 & y_2 & z_2 \\ x_3 & y_3 & z_3 \\ x_4 & y_4 & z_4 \end{bmatrix}, \quad b_1 = \det\begin{bmatrix} y_2 & z_2 & 1 \\ y_3 & z_3 & 1 \\ y_4 & z_4 & 1 \end{bmatrix}$$
$$c_1 = \det\begin{bmatrix} z_2 & 1 & x_2 \\ z_3 & 1 & x_3 \\ z_4 & 1 & x_4 \end{bmatrix}, \quad d_1 = \det\begin{bmatrix} 1 & x_2 & y_2 \\ 1 & x_3 & y_3 \\ 1 & x_4 & y_4 \end{bmatrix} \tag{5.24b}$$

with the other constants defined by cyclic interchange of the subscripts in the order 1, 2, 3, 4. This gives the shape functions

$$N_a(x, y, z) = \frac{1}{6V}\left(a_a + b_a x + c_a y + d_a z\right), \quad a = 1, 2, 3, 4 \tag{5.25}$$

Integrals to compute element matrices may be carried out using results in Appendix E.

In the next chapter we shall generalize the above element forms to permit a systematic development with polynomials of any degree, as well as to permit curved edges. The above forms, however, provide a basis from which we can consider solutions to a number of different problem forms for the quasi-harmonic equation. We begin by describing the element matrices for the simple triangular element.

Example 5.1. Element arrays for plane three-node triangular element

With shape functions written in the form

$$N_a = \frac{a_a + b_a x + c_a y}{2\Delta}$$

in which Δ and a_a, b_a, c_a are defined in Section 5.1.3, the computation of the "mass" matrix, $\mathbf{C}^e$, is given by

$$C^e_{ab} = \int_\Delta N_a c N_b h_z \, \mathrm{d}x \, \mathrm{d}y$$

which for c constant over the element gives

$$\mathbf{C}^e = \frac{c h_z \Delta}{12}\begin{bmatrix} 2 & 1 & 1 \\ 1 & 2 & 1 \\ 1 & 1 & 2 \end{bmatrix}$$

This result may be computed using the exact expression given in Appendix E.

The derivatives of the shape functions are expressed as

$$\frac{\partial N_a}{\partial x} = \frac{b_a}{2\Delta}, \qquad \frac{\partial N_a}{\partial y} = \frac{c_a}{2\Delta}$$

giving the gradient matrix

$$\mathbf{b}_a = \frac{1}{2\Delta}\begin{bmatrix} b_a & c_a \end{bmatrix}^{\mathrm{T}}$$

Since the gradient matrix is constant the element "stiffness" matrix (ignoring the H boundary term) is given by (noting $k_{xy} = k_{yx}$)

$$\mathbf{H}^e = \left\{ \frac{k_{xx}}{4\Delta} \begin{bmatrix} b_1b_1 & b_1b_2 & b_1b_3 \\ b_2b_1 & b_2b_2 & b_2b_3 \\ b_3b_1 & b_3b_2 & b_3b_3 \end{bmatrix} + \frac{k_{yy}}{4\Delta} \begin{bmatrix} c_1c_1 & c_1c_2 & c_1c_3 \\ c_2c_1 & c_2c_2 & c_2c_3 \\ c_3c_1 & c_3c_2 & c_3c_3 \end{bmatrix} + \frac{k_{xy}}{4\Delta} \begin{bmatrix} (b_1c_1 + c_1b_1) & (b_1c_2 + c_1b_2) & (b_1c_3 + c_1b_3) \\ (b_2c_1 + c_2b_1) & (b_2c_2 + c_2b_2) & (b_2c_3 + c_2b_3) \\ (b_3c_1 + c_3b_1) & (b_3c_2 + c_3b_2) & (b_3c_3 + c_3b_3) \end{bmatrix} \right\} h_z$$

The load matrices follow a similar simple pattern and thus, for instance, due to constant Q we have

$$s_a^e = \int_\Delta N_a Q h_z \, \mathrm{d}x \, \mathrm{d}y = \frac{1}{3} Q h_z \Delta$$

This is a very simple (almost "obvious") result.

Example 5.2. "Stiffness" matrix for axisymmetric three-node triangular element

The computation of the arrays for an axisymmetric problem involves an integral of the radius over the area of the triangle. This is given by [viz. Appendix E]

$$\int_\Delta r \, \mathrm{d}r \, \mathrm{d}z = \bar{r}\Delta$$

where $\bar{r} = (r_1 + r_2 + r_3)/3$. This then gives the results

$$\mathbf{H}^e = \left\{ \frac{k_{rr}}{4\Delta} \begin{bmatrix} b_1b_1 & b_1b_2 & b_1b_3 \\ b_2b_1 & b_2b_2 & b_2b_3 \\ b_3b_1 & b_3b_2 & b_3b_3 \end{bmatrix} + \frac{k_{zz}}{4\Delta} \begin{bmatrix} c_1c_1 & c_1c_2 & c_1c_3 \\ c_2c_1 & c_2c_2 & c_2c_3 \\ c_3c_1 & c_3c_2 & c_3c_3 \end{bmatrix} + \frac{k_{rz}}{4\Delta} \begin{bmatrix} (b_1c_1 + c_1b_1) & (b_1c_2 + c_1b_2) & (b_1c_3 + c_1b_3) \\ (b_2c_1 + c_2b_1) & (b_2c_2 + c_2b_2) & (b_2c_3 + c_2b_3) \\ (b_3c_1 + c_3b_1) & (b_3c_2 + c_3b_2) & (b_3c_3 + c_3b_3) \end{bmatrix} \right\} 2\pi\bar{r}$$

Example 5.3. Load matrix for axisymmetric three-node triangular element

The nodal forces from a constant source term Q are computed from

$$s_a^e = \int_\Delta N_a Q 2\pi r_b N_b \, \mathrm{d}r \, \mathrm{d}z$$

and thus now has quadratic terms in the coordinates. If we substitute

$$r = \bar{r} + x$$

and use the results from Appendix E we obtain for node 1

$$s_1^e = \frac{1}{6}(2r_1 + r_2 + r_3)\pi Q \Delta$$

with results for s_2^e and s_3^e obtained by cyclic permutation.

5.2 Partial discretization: Transient problems

The transient problem may be solved in a number of ways. In Chapter 3 we considered a simple discrete time method for the one-dimensional problem in terms of the rate. We again consider the procedure described in Section 3.9.3 in which the time dependence is given by (3.96). However, here we will formulate our solution in terms of the discrete values of ϕ itself. If we let

$$\widehat{\boldsymbol{\phi}}_{n+1} = \tilde{\boldsymbol{\phi}}_n + (1-\theta)\Delta t \dot{\tilde{\boldsymbol{\phi}}}_n$$

denote all the terms from the solution at time t_n, from (3.96) the approximation to the rate at t_{n+1} is given by

$$\dot{\tilde{\boldsymbol{\phi}}}_{n+1} = \frac{1}{\theta\,\Delta t}\left(\tilde{\boldsymbol{\phi}}_{n+1} - \widehat{\boldsymbol{\phi}}_{n+1}\right)$$

where $\Delta t = t_n - t_{n-1}$ and $\theta > 0$. An approximate solution to the semi-discrete equations at each time t_{n+1} is obtained by solving the set of equations

$$\left[\frac{1}{\theta\,\Delta t}\mathbf{C} + \mathbf{H}\right]\tilde{\boldsymbol{\phi}}_{n+1} = \mathbf{s}_{n+1} + \frac{1}{\theta\,\Delta t}\mathbf{C}\widehat{\boldsymbol{\phi}}_{n+1} \tag{5.26}$$

If the initial condition is approximated as

$$\phi(\mathbf{x}, 0) \approx \mathbf{N}(\mathbf{x})\tilde{\boldsymbol{\phi}}(0) \qquad \text{with } \tilde{\boldsymbol{\phi}}(0) = \tilde{\boldsymbol{\phi}}_0$$

a solution for $\tilde{\boldsymbol{\phi}}_1$ is immediately available from (5.26) by solving a set of *algebraic equations*. For each subsequent time step the solution process is identical to the time-independent problem except for the modified force vector and a need to use a coefficient matrix which has a term inversely proportional to the size of the time increment.

5.3 Numerical examples: An assessment of accuracy

Assembling explicitly worked out "stiffnesses" of triangular elements for the "regular" mesh pattern shown in Fig. 5.5a the discretized equations are *identical* with those that are derived by well-known finite difference methods [49]. The same result holds for the mesh pattern shown in Fig. 5.5b [10]. For cases where all boundary conditions are given as prescribed values

$$\phi = \bar{\phi} \qquad \text{on } \Gamma_\phi$$

the solutions obtained by the two methods obviously will be identical, and so also will be the orders of approximation.

However, if the mesh shown in Fig. 5.5c, which is also based on a square arrangement of nodes but with an "irregular" element pattern, is used a difference between the two approaches for the "load" vector $\mathbf{s}^e$ will be evident. The assembled equations will have the same "stiffness" matrix as in Fig. 5.5a but will show "loads" which

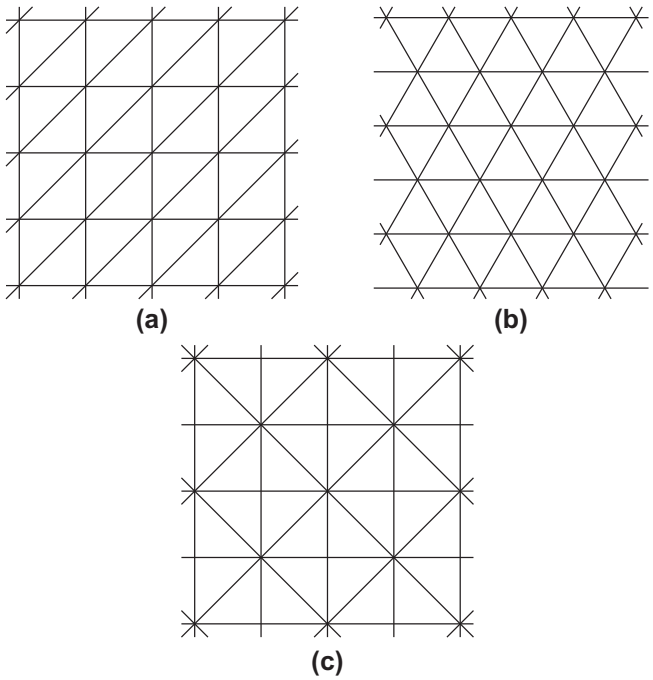

FIGURE 5.5
"Regular" and "irregular" subdivision patterns.

differ by small amounts from node to node, the sum of the loads is still the same as that due to the finite difference expressions. The solutions therefore differ only locally and will represent the same averages.

Further advantages of the finite element process are:

1. It can deal simply with nonhomogeneous and anisotropic situations (particularly when the direction of anisotropy is variable).
2. The elements can be graded in shape and size to follow arbitrary boundaries and to allow for regions of rapid variation of the function sought, thus controlling the errors in a most efficient way (viz. Chapters 15 and 16).
3. Specified gradient or "radiation" boundary conditions are introduced naturally and with a better accuracy than in standard finite difference procedures.
4. Higher order elements presented in the next chapter can be readily used to improve accuracy without complicating boundary conditions—a difficulty always arising with finite difference approximations of a higher order.
5. Finally, but of considerable importance in the computer age, standard programs may be used for assembly and solution.

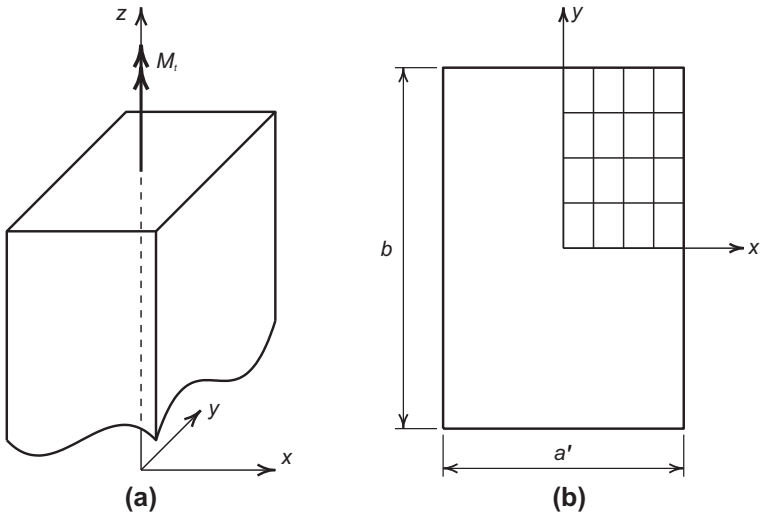

FIGURE 5.6
Torsion of rectangular prismatic bar.

5.3.1 Torsion of prismatic bars

The torsion of prismatic elastic bars may be solved using a quasi-harmonic equation formulation. Here either a *warping function* or a *stress function* approach may be used. In Fig. 5.6a we show a rectangular bar loaded by an end torque M_t. The analysis is performed on the cross-section as shown in Fig. 5.6b.

The use of a warping function is governed by the formulation in which displacements are given as

$$u = -yz\theta, \qquad v = xz\theta, \qquad \text{and} \qquad w = \psi(x, y)\theta$$

where x, y are coordinates in the cross-section, z is a coordinate of the bar axis, θ is the rate of twist, and ψ is the warping function. The nonzero strain components resulting from these displacements are given by

$$\gamma_{xz} = \theta\left(\frac{\partial\psi}{\partial x} - y\right) \qquad \text{and} \qquad \gamma_{yz} = \theta\left(\frac{\partial\psi}{\partial y} + x\right) \tag{5.27}$$

giving, for an isotropic elastic material, the nonzero stresses

$$\tau_{xz} = G\gamma_{xz} \qquad \text{and} \qquad \tau_{yz} = G\gamma_{yz} \tag{5.28}$$

Inserting the expression for stresses into the equilibrium equation (2.18) with zero body and inertia forces gives the governing differential equation

$$\theta\left[\frac{\partial}{\partial x}\left(G\frac{\partial\psi}{\partial x}\right) + \frac{\partial}{\partial y}\left(G\frac{\partial\psi}{\partial y}\right)\right] = 0 \tag{5.29}$$

and for stress-free boundary conditions

$$\tau_{nz} = n_x \tau_{xz} + n_y \tau_{yz} = 0 \tag{5.30}$$

in which n_x and n_y are the direction cosines for the outward normal to the boundary of the rectangular section. Thus, for $\theta G = k_{xx} = k_{yy}, k_{xy} = 0$ we have the standard quasi-harmonic equation. Introducing appropriate changes in parameter definitions into (5.7), the problem is solved from the weak form expressed as

$$\mathrm{G}(\delta\psi, \psi) = \theta \int_\Omega \left[\frac{\partial \delta\psi}{\partial x} G \left(\frac{\partial \psi}{\partial x} - y \right) + \frac{\partial \delta\psi}{\partial y} G \left(\frac{\partial \psi}{\partial y} + x \right) \right] \mathrm{d}\Omega = 0$$

At least one value of the warping function must be specified to have a unique solution. In addition a unit value of θ may be used in G during computation of ψ. In this case the element s_a is given by

$$s_a = \int_\Omega \left(\frac{\partial N_a}{\partial x} y - \frac{\partial N_a}{\partial y} x \right) \mathrm{d}\Omega$$

The total torque acting on a cross-section is given by

$$\begin{aligned} M_t &= \int_A \left[-\tau_{xz} y + \tau_{yz} x \right] \mathrm{d}A \\ &= \int_A G \left[x^2 + y^2 - y \frac{\partial \psi}{\partial x} + x \frac{\partial \psi}{\partial y} \right] \mathrm{d}A \, \theta = \overline{GJ}_\psi \theta \end{aligned}$$

where $\overline{GJ}_\psi$ is the effective torsional stiffness.

As an alternative a stress function formulation is deduced using the representation for stresses

$$\tau_{xz} = -\frac{\partial \phi}{\partial y} \quad \text{and} \quad \tau_{yz} = \frac{\partial \phi}{\partial x} \tag{5.31}$$

Combining (5.27) and (5.28) with (5.31) and eliminating the warping function ψ gives the differential equation

$$\frac{\partial}{\partial x} \left(\frac{1}{G} \frac{\partial \phi}{\partial x} \right) + \frac{\partial}{\partial y} \left(\frac{1}{G} \frac{\partial \phi}{\partial y} \right) = 2\theta$$

with

$$\phi(s) = \text{Constant} \qquad \text{on } \Gamma_q$$

representing a stress-free boundary condition.

The total torque acting on a cross-shaded section is now given by

$$M_t = \int_A \left[x \frac{\partial \phi}{\partial x} + y \frac{\partial \phi}{\partial y} \right] \mathrm{d}A = \overline{GJ}_\phi \theta$$

where $\overline{GJ}_\phi$ is the effective torsional stiffness.

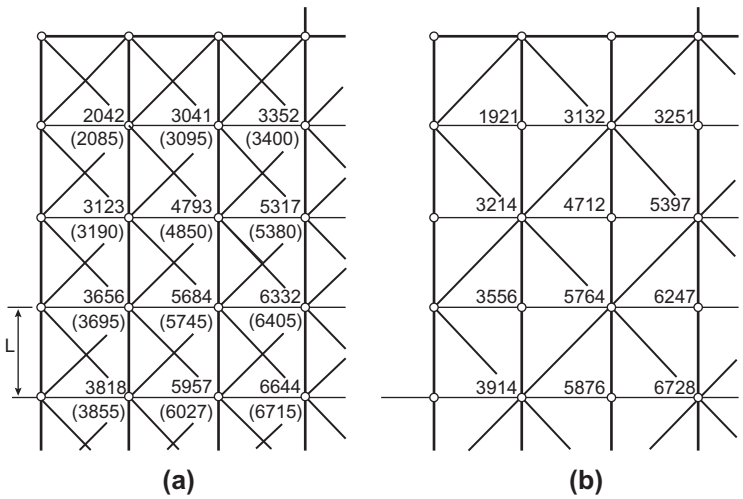

FIGURE 5.7
Torsion of a rectangular shaft. The numbers in parentheses show a more accurate solution due to Southwell using a 12×16 mesh (values of $\phi/G\theta L^2$).

The two solutions provide a bound on the torsional stiffness with the warping function solution giving an upper bound, $\overline{GJ}_\psi$, and the stress function a lower bound, $\overline{GJ}_\phi$.

5.3.1.1 *Torsion of rectangular shaft*

In Fig. 5.7 a test comparing the results obtained on an "irregular" mesh of three-node triangular elements with a relaxation solution of the lowest order finite difference approximation is shown. Both give results of similar accuracy, as indeed would be anticipated. In general superior accuracy is available with the finite element discretization. Furthermore, it is possible to get bounds on the torsional stiffness, as indicated above. To illustrate this latter aspect we consider a square bar which is solved using four-node rectangular elements and a range of $n \times n$ meshes in which n is the number of spaces between nodes on each side. The results for the computed torsional stiffness values are plotted in Fig. 5.8.

5.3.1.2 *Torsion of hollow bimetallic shaft*

The pure torsion of a nonhomogeneous rectangular shaft with a circular hole is illustrated in Fig. 5.9. In the finite element solution presented, the hollow section is represented by a material for which G has a value of the order of 10^{-3} compared with the other materials.[1] The results compare well with the contours derived from an accurate finite difference solution [11].

[1]This was done to avoid difficulties due to the "multiple connection" of the region and to permit the use of a standard program.

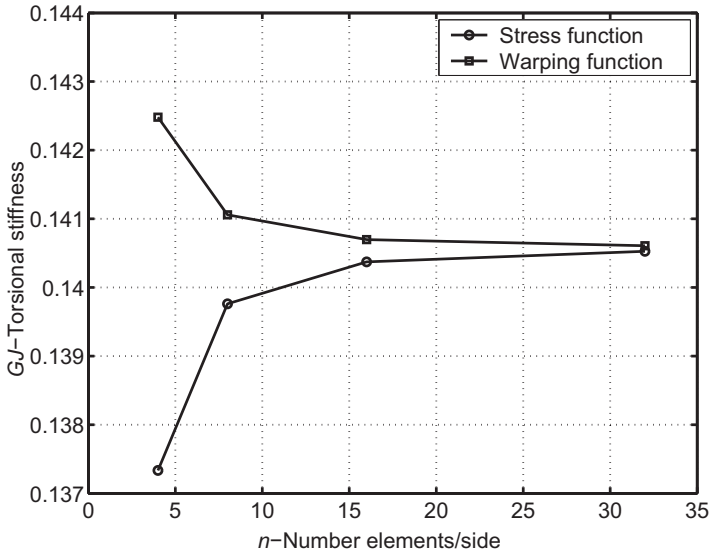

FIGURE 5.8

Bound on torsional stiffness for square bar.

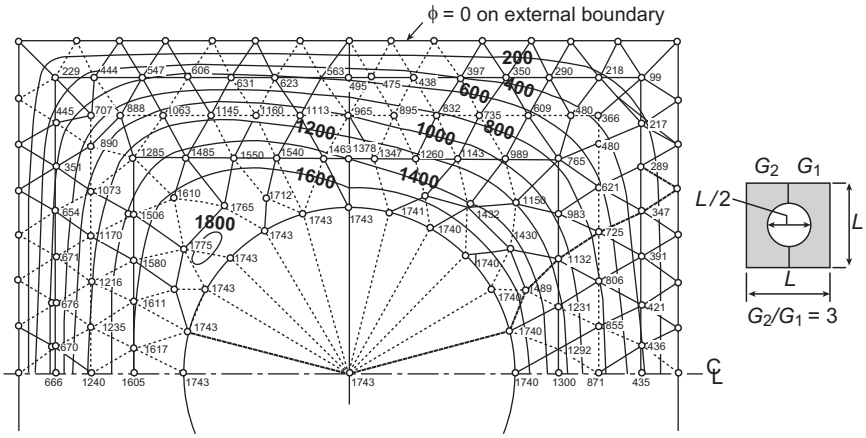

FIGURE 5.9

Torsion of a hollow bimetallic shaft. $\phi/G\theta L^2 \times 10^4$.

5.3.2 Transient heat conduction

5.3.2.1 Transient heat conduction of a rectangular bar

Consider a long bar with a square cross-section of size $L \times L$ in which the transient heat conduction equation (2.84) applies and assume that the rate of heat generation

varies with time as

$$Q = Q_0 \, \mathrm{e}^{-\alpha t} \tag{5.32}$$

(this might approximate a problem of heat development due to hydration of concrete). We assume that at $t = 0, \phi = 0$ throughout. Further, we shall take $\phi = 0$ on all boundaries for all times.

A Fourier series approximation for the solution is given by

$$\begin{aligned} \phi &= \sum_{m=1}^{M} \sum_{n=1}^{N} N_{mn}(x, y) \tilde{\phi}_{mn}(t) \\ N_{mn} &= \cos \frac{m\pi x}{L} \cos \frac{n\pi y}{L}, \quad m, n = 1, 3, 5, \ldots \end{aligned} \tag{5.33}$$

with x and y measured from the center (Fig. 5.10). The even components of the Fourier series are omitted due to the required symmetry of solution. When substituted into the weak form only diagonal terms exist in $\mathbf{H}$ and $\mathbf{C}$, and we have

$$\begin{aligned} H_{mn} &= \int_{-L/2}^{L/2} \int_{-L/2}^{L/2} \left[k \left(\frac{\partial N_{mn}}{\partial x} \right)^2 + k \left(\frac{\partial N_{mn}}{\partial y} \right)^2 \right] \mathrm{d}x \, \mathrm{d}y = \frac{\pi^2 k}{4} (m^2 + n^2) \\ C_{mn} &= \int_{-L/2}^{L/2} \int_{-L/2}^{L/2} c N_{mn}^2 \, \mathrm{d}x \, \mathrm{d}y = \frac{L^2 c}{4} \\ s_{mn} &= \int_{-L/2}^{L/2} \int_{-L/2}^{L/2} N_{mn} Q_0 \, \mathrm{e}^{-\alpha t} \, \mathrm{d}x \, \mathrm{d}y \\ &= \frac{4 Q_0 L^2}{mn\pi^2} (-1)^{(m+3)/2} (-1)^{(n+3)/2} \, \mathrm{e}^{-\alpha t} \end{aligned} \tag{5.34}$$

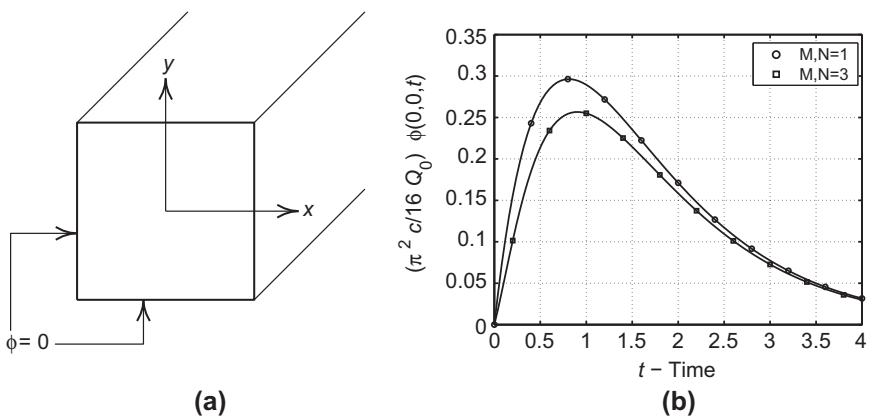

FIGURE 5.10
Two-dimensional transient heat development in a square prism—plot of temperature at center: (a) boundary condition and (b) solution at center.

This leads to an ordinary differential equation with parameters $\tilde{\phi}_{mn}$:

$$H_{mn}\tilde{\phi}_{mn} + C_{mn}\frac{\mathrm{d}\tilde{\phi}_{mn}}{\mathrm{d}t} + s_{mn} = 0 \tag{5.35}$$

with initial condition $\tilde{\phi}_{mn} = 0$ when $t = 0$. The exact solution of this is easy to obtain, as is shown in Fig. 5.10 for the parameters

$$L = c = Q_0 = \alpha = 1 \qquad \text{and} \qquad k = \frac{0.75}{\pi^2}$$

and choices for M and N.

The above solution also may be used to assess the accuracy of a finite element result. For the finite element solution we use four-node square elements. The transient solution is performed using the procedure given in Section 5.2. Using symmetry conditions, a mesh of 20×20 four-node elements is used to approximate one quadrant of the domain. A constant increment in time, $\Delta t = 0.01$, is used to perform the solution. Results for the temperature at the center of the prism are given in Fig. 5.11 and compared to the series solutions.

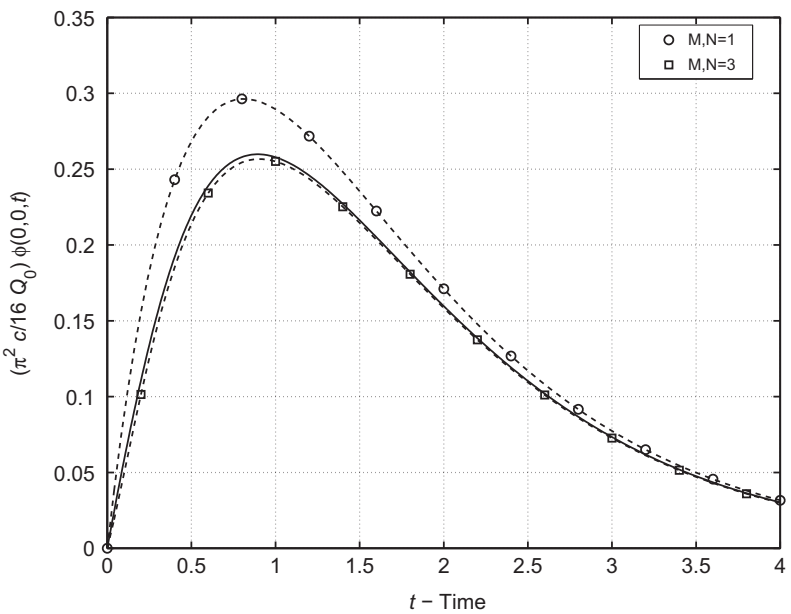

FIGURE 5.11
Transient heat development in a square prism—plot of temperature at center.

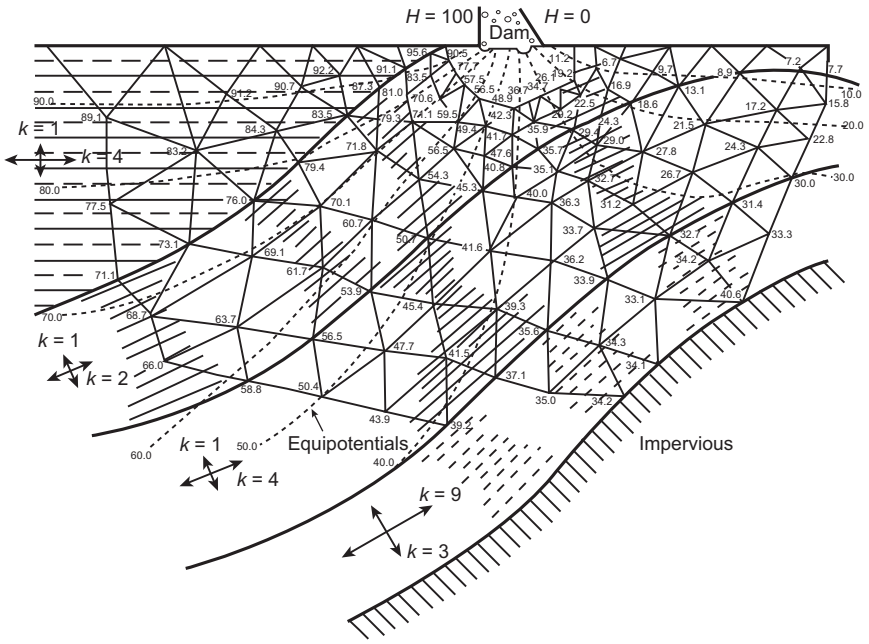

FIGURE 5.12
Flow under a dam through a highly nonhomogeneous and contorted foundation.

5.3.3 Anisotropic seepage

The next problem is concerned with the flow through highly nonhomogeneous, anisotropic, and contorted strata. The basic governing equation is

$$\frac{\partial}{\partial x'}\left(k_{x'x'}\frac{\partial H}{\partial x'}\right)+\frac{\partial}{\partial y'}\left(k_{y'y'}\frac{\partial H}{\partial y'}\right)=0 \tag{5.36}$$

in which H is the hydraulic head and $k_{x'x'}$ and $k_{y'y'}$ represent the permeability coefficients in the direction of the (inclined) principal axes. However, a special feature has to be incorporated to allow for changes of x' and y' principal directions from element to element.

No difficulties are encountered in computation, and the problem together with its solution is given in Fig. 5.12 [3].

5.3.4 Electrostatic and magnetostatic problems

In this area of activity frequent need arises to determine appropriate field strengths and the governing equations are commonly of the standard quasi-harmonic type discussed here. Thus the formulations are directly transferable. One of the first applications made as early as 1967 [4] was to fully three-dimensional electrostatic field distributions governed by simple Laplace equations (Fig. 5.13).

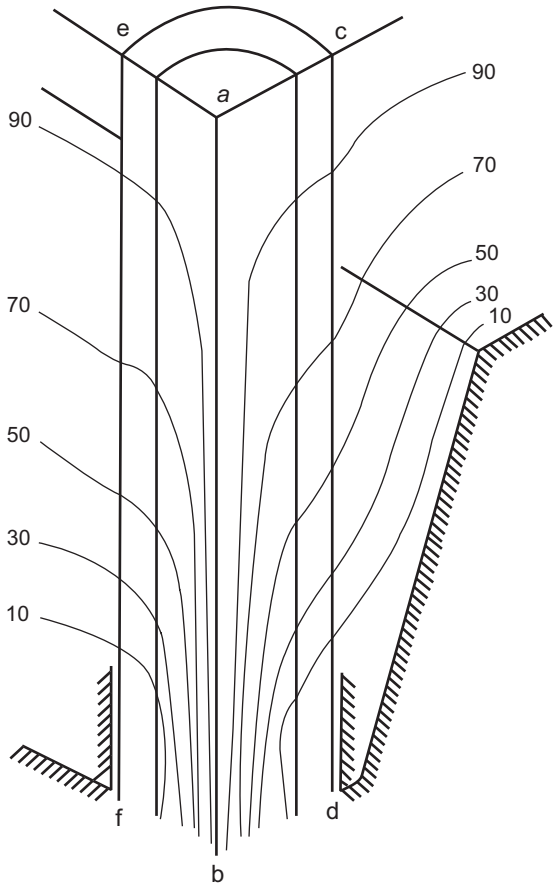

FIGURE 5.13
A three-dimensional distribution of electrostatic potential around a porcelain insulator in an earthed trough.

In Fig. 5.14 a similar use of triangular elements was made in the context of magnetic two-dimensional fields by Winslow [6]. These early works stimulated considerable activity in this area and much additional work has been published [12–15].

5.3.5 Lubrication problems

Once again a standard Poisson type of equation is encountered in the two-dimensional domain of a bearing pad. In the simplest case of constant lubricant density and viscosity the equation to be solved is the Reynolds equation

$$\frac{\partial}{\partial x}\left(h^3\frac{\partial p}{\partial x}\right)+\frac{\partial}{\partial y}\left(h^3\frac{\partial p}{\partial y}\right)=6\mu V\frac{\partial h}{\partial x} \tag{5.37}$$

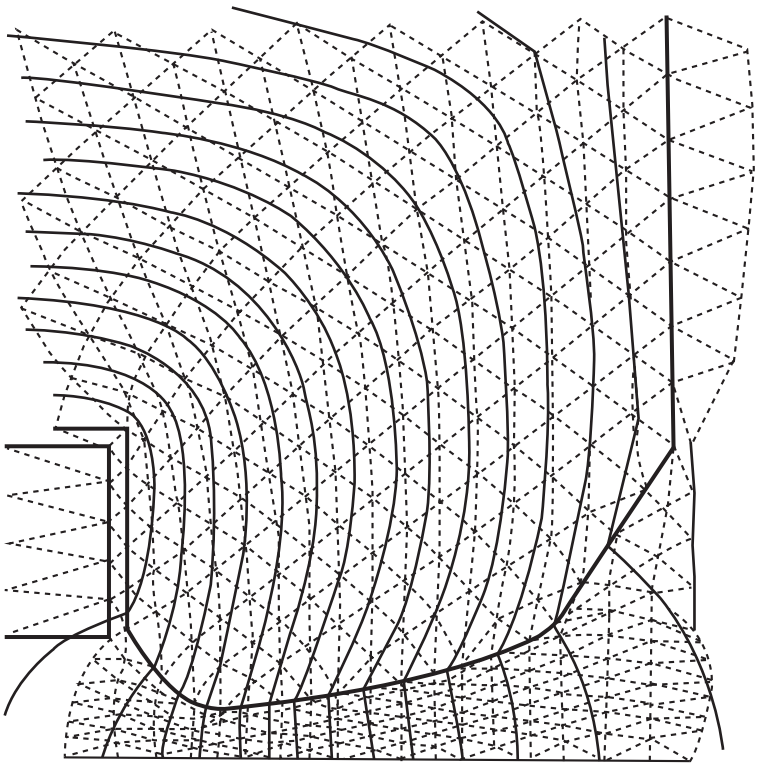

FIGURE 5.14
Field near a magnet.

where h is the film thickness, p is the pressure developed, μ is the viscosity, and V is the velocity of the pad in the x-direction.

Figure 5.15 shows the pressure distribution in a typical finite width stepped pad [16]. The boundary condition is simply that of zero pressure and it is of interest to note that the step causes an equivalent of a "line load" on integration by parts of the right-hand side of Eq. (5.37).

More general cases of lubrication problems, including vertical pad movements (squeeze films) and compressibility, can obviously be dealt with, and much work has been done here [17–25].

5.3.6 Irrotational and free surface flows

The basic Laplace equation which governs the flow of viscous fluid in seepage problems is also applicable in the problem of irrotational fluid flow outside the boundary layer created by viscous effects. The seepage example given above is adequate to illustrate the general applicability in this context. Further examples for this class of problems are cited by Martin [26] and others [25,27–32].

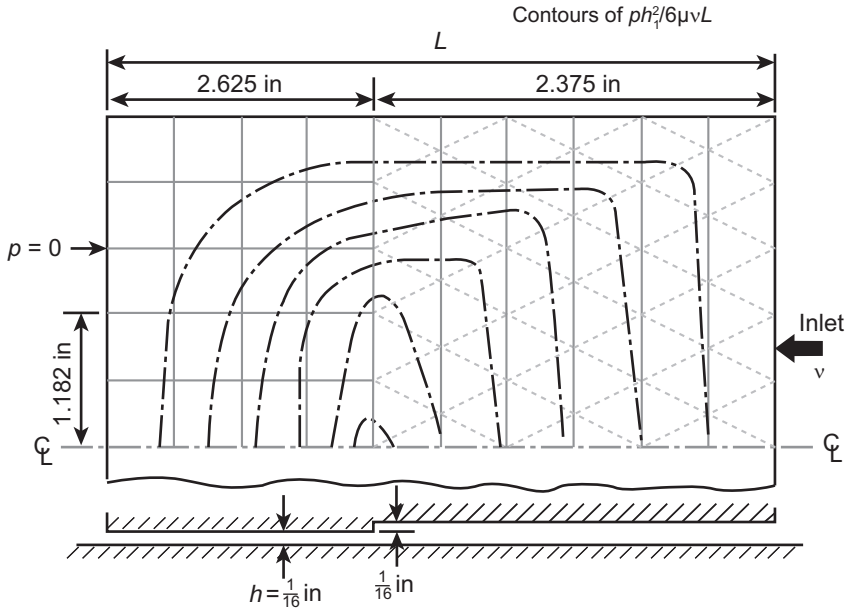

FIGURE 5.15
Pressure distribution for a stepped pad bearing.

If no viscous effects exist, then it can be shown that for a fluid starting at rest the motion must be irrotational, i.e.,

$$\omega_z \equiv \frac{\partial u}{\partial y} - \frac{\partial v}{\partial x} = 0 \tag{5.38}$$

where u and v are appropriate velocity components.

This implies the existence of a velocity potential, giving

$$u = -\frac{\partial \phi}{\partial x}, \qquad v = -\frac{\partial \phi}{\partial y} \tag{5.39a}$$

or

$$\mathbf{u} = -\nabla \phi \tag{5.39b}$$

If, further, the flow is incompressible, the continuity equation [which is similar to Eq. (2.80)] has to be satisfied, i.e.,

$$\nabla^{\mathrm{T}} \mathbf{u} = 0 \tag{5.40}$$

and therefore

$$\nabla^{\mathrm{T}} (\nabla \phi) = \nabla^2 \phi = 0 \tag{5.41}$$

Alternatively, for two-dimensional flow a stream function may be introduced defining the velocities as

$$u = -\frac{\partial \psi}{\partial y}, \qquad v = \frac{\partial \psi}{\partial x} \tag{5.42}$$

and this identically satisfies the continuity equation. The irrotational condition must now ensure that

$$\nabla^{\mathrm{T}}(\nabla\psi) = \nabla^2\psi = 0 \tag{5.43}$$

and thus problems of ideal fluid flow can be posed in either form. As the standard formulation is again applicable, there is little more that needs to be added, and for examples the reader can consult the literature cited. We also discuss this problem in more detail in Ref. [33].

The similarity with problems of seepage flow, which has already been discussed, is obvious [34,35].

A particular class of fluid flow deserves mention. This is the case when a free surface limits the extent of the flow and this surface is not known *a priori*.

The class of problem is typified by two examples—that of a freely overflowing jet (Fig. 5.16a) and that of flow through an earth dam (Fig. 5.16b). In both, the free surface represents a streamline and in both the position of the free surface is unknown *a priori* but has to be determined so that an *additional condition* on this surface is satisfied. For instance, in the second problem, if formulated in terms of the potential for the hydraulic head H, Eq. (5.36) governs the problem.

The free surface, being a streamline, imposes the condition that

$$\frac{\partial H}{\partial n} = 0 \tag{5.44}$$

be satisfied there. In addition, however, the pressure must be zero on the surface as this is exposed to atmosphere. As

$$H = \frac{p}{\gamma} + y \tag{5.45}$$

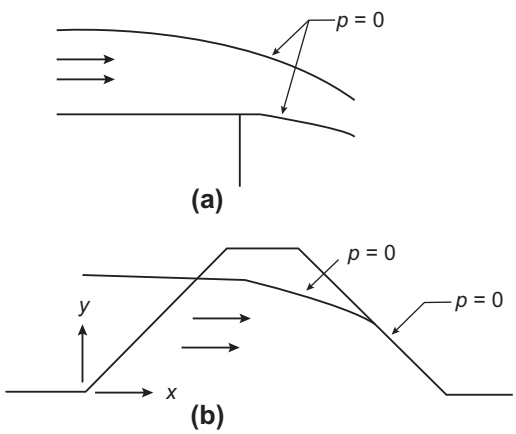

FIGURE 5.16
Typical free surface problems with a streamline also satisfying an additional condition of pressure = 0: (a) jet overflow and (b) seepage through an earth dam.

where γ is the fluid specific weight, p is the fluid pressure, and y is the elevation above some (horizontal) datum, we must have on the surface

$$H = y \tag{5.46}$$

The solution may be approached iteratively. Starting with a prescribed free surface streamline the standard problem is solved. A check is carried out to see if Eq. (5.46) is satisfied and, if not, an adjustment of the surface is carried out to make the new y equal to the H just found. A few iterations of this kind show that convergence is reasonably rapid. Taylor and Brown [36] show such a process. Alternative methods including special variational principles for dealing with this problem have been devised over the years and interested readers can consult Refs. [37–45].

5.4 Problems

5.1 The anisotropic properties for $\mathbf{k}$ are $k_{x'} = 0.4$, $k_{y'} = 2.1$, and $k_{z'} = 1.0$. The axes are oriented as shown in Fig. 5.17. For $\theta = 30°$ compute the terms in the matrix $\mathbf{k}$ (e.g., k_{xx}, k_{xy}, etc.) with respect to the axes x, y, z.

5.2 A two-dimensional heat equation is located in the x-y plane. The problem is allowed to convect heat to the surrounding region according to

$$Q(x, y) = -\beta[\phi(x, y) - \phi_0]$$

where β is a convection parameter and ϕ_0 the temperature of the surrounding medium.

Construct a weak form for the problem.

For a finite element approximation to ϕ and $\delta\phi$ deduce the form of the new matrices which result from the modified weak form.

5.3 For the quasi-harmonic equation consider a square four-node element with unit side lengths in the x- and y-directions. Using *FEAPpv* (or any other available

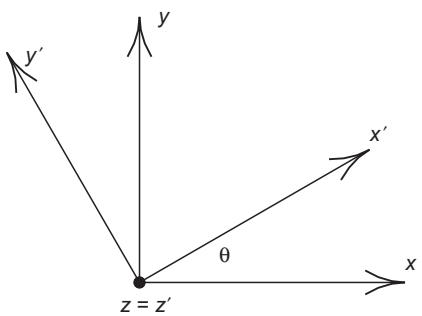

FIGURE 5.17
Orientation of axes for Problem 5.1.

program) determine the rank of the element matrix $\mathbf{H}$ for the case where $\mathbf{k} = \mathbf{I}$ (i.e., isotropic with $k = 1$) and $H = 0$ using 1×1 Gaussian quadrature. Repeat the calculation using 2×2 and 3×3 quadrature where each direction uses the values given in Table 3.3:

(a) What is the lowest order quadrature that gives a matrix $\mathbf{H}$ with full rank?
(b) What is the lowest order quadrature that evaluates the matrix $\mathbf{H}$ exactly?

Hint: The rank of $\mathbf{H}$ may be determined from the eigenproblem given by

$$\mathbf{H}\mathbf{v}_i = \lambda_i \mathbf{v}_i \qquad \text{with } \mathbf{v}_i^{\mathrm{T}} \mathbf{v}_j = \delta_{ij}$$

where δ_{ij} is the Kronecker delta. The rank of $\mathbf{H}$ is the number of nonzero eigenvalues λ_i (a zero is any value below the round-off limit).

5.4 Solve Problem 5.3 for a three-node triangular element mesh.
Using the eigenvector for the zero eigenvalue of the fully integrated element array $\mathbf{H}$ determine and sketch the shape of eigenvectors for the nonzero eigenvalues. (Note: The element has one zero eigenvalue, $\mathbf{v}_0$.)

5.5 Consider the torsion of a rectangular bar by the warping function formulation discussed in Section 5.3.1. Let a and b be the side lengths in the x- and y-directions, respectively. For a homogeneous section with shear modulus G the warping function has the behavior shown in Fig. 5.18 for a/b ratios of 1, 1.25, and 2. Note that the behavior transitions from eight to four regions of $\pm$ variation. Estimate the a/b ratio where this transition just occurs.
To make your estimate use *FEAPpv* (or any other available program) with a fine mesh of four-node rectangular elements. Set the boundary conditions to make the warping function zero along the x and y axes. The transition will occur at the smallest a/b for which all the values on the perimeter of one quadrant of the cross-section have the same sign or are "numerically" zero.

5.6 A cross-section of a long prismatic section is shown in Fig. 5.19 and subjected to a constant uniform temperatures 370 °C on the left boundary and 66 °C on the right boundary. The top and bottom edges are assumed to be insulated so that $q_n = 0$.

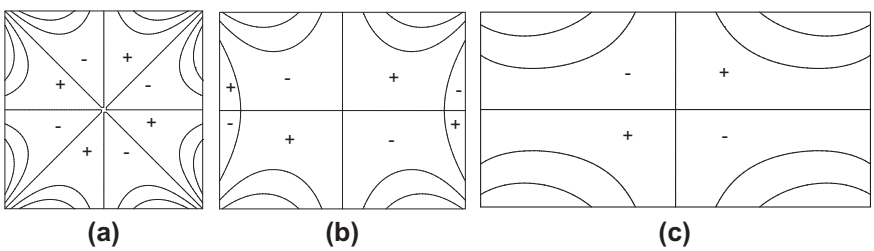

FIGURE 5.18
Warping function for torsion of rectangular bar for Problem 5.5: (a) $a/b = 1$; (b) $a/b = 1.25$; (c) $a/b = 2$.

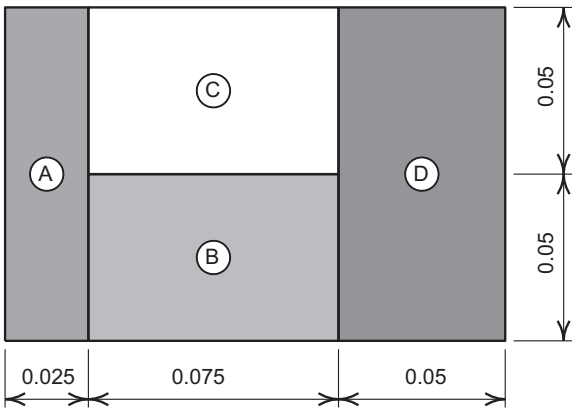

FIGURE 5.19
Thermal analysis of composite section for Problem 5.6.

The cross-section is a composite of fir (A), concrete (B), glass wool (C), and yellow pine (D). The thermal conductivity for each of the parts is $k_A = 0.11$, $k_B = 0.78$, $k_C = 0.04$, and $k_D = 0.147$ in consistent units for the geometry of the section shown:

(a) Estimate the heat flow through the cross-section assuming $q_y = 0$ and q_x is constant in each part. Let the temperatures at each junction be $T(0) = 370$, $T(0.025) = T_1$, $T(0.10) = T_2$, and $T(0.15) = 66$.
Hint: Assume T is a function of x only.

(b) Use *FEAPpv* (or any other available program) to compute a finite element solution using four-node rectangular elements. First perform a solution on a coarse mesh and use this to design a mesh using a finer discretization.

Plot a distribution of heat flow q_n across each of the internal boundaries.

5.7 Company X&Y plans to produce a rectangular block which needs to be processed by a thermal quench in a medium which is 100 °C above room temperature. The block shown in Fig. 5.20a has $a = 10$ and $b = 20$ (i.e., the block is $10 \times 10 \times 20$). It has been determined that the thermal properties of the block may be specified by an isotropic Fourier model in which $k = 1$ and $c = 1$. The surface convection constant H is 0.05.
The quench must be maintained until the minimum temperature in the block reaches 99 °C above room temperature. Use *FEAPpv* (or any other available program) to perform a transient analysis to estimate the required quench time:

(a) First perform a 2-D plane analysis on a 10×10 cross-section using a uniform mesh of four-node quadrilateral elements. Use symmetry to reduce the size of the domain analyzed. The surface convection will be modeled by two-node line elements along the outer perimeter. The analysis region is shown in Fig. 5.20b with the boundary conditions to be imposed. Locate

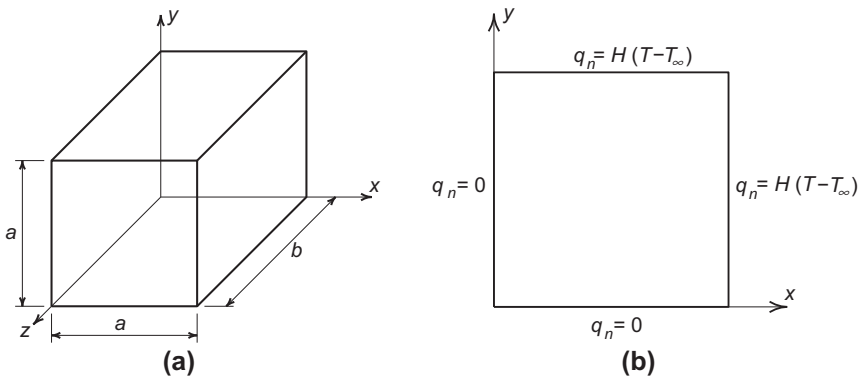

FIGURE 5.20
Thermal quench in two and three dimensions for Problem 5.7.

the node where the minimum temperature occurs and plot the behavior vs. time (a good option is to use MATLAB or GNU Octave to perform plots). Estimate the duration of time needed for the minimum temperature to reach the desired value. (Hint: One approach to selecting time increments is to select a very small value, e.g., $\Delta t = 10^{-8}$ and perform 10 steps of the solution. Multiply the time increment by 10 and perform 9 more steps. Repeat the multiplication until the desired final time value is reached.)

(b) Using the time duration estimated in (a) perform a 3-D analysis using a uniform mesh of eight-node hexahedral elements. Use symmetry to reduce the size of the region analyzed. Note: The convection condition applies to all outer surfaces.
Estimate the duration of quench time needed for the minimum temperature to reach the desired value.

(c) What analyses would you perform if the block was $10 \times 10 \times 5$?

(d) Comment on use of a 2-D analysis to estimate the required quench times for other part shapes.

5.8 The distribution of shear stresses on the cross-section of a cantilever beam shown in Fig. 5.21a may be determined by solving the quasi-harmonic equation [46]

$$\frac{\partial^2 \phi}{\partial x^2} + \frac{\partial^2 \phi}{\partial y^2} = 0$$

with boundary condition

$$\phi = \frac{P}{2I}\left[\int y^2 \mathrm{d}x - \frac{\nu}{3(1+\nu)} y^3\right]$$

where P is the end load, I is the moment of inertia of the cross-section, ν is the Poisson ratio of an isotropic elastic material, and ϕ is a stress function. The

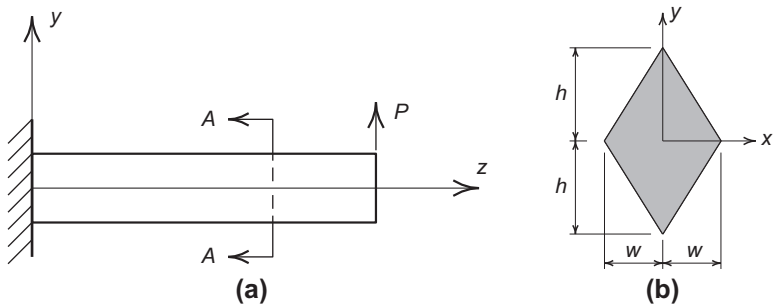

FIGURE 5.21
End-loaded cantilever beam for Problem 5.8: (a) cantilever beam and (b) section A-A.

shear stresses are determined from

$$\tau_{xz} = -\frac{\partial \phi}{\partial y} \quad \text{and} \quad \tau_{yz} = \frac{\partial \phi}{\partial x} + \frac{P}{2I}\left[\frac{\nu}{1+\nu}x^2 - y^2\right]$$

See Ref. [46] for details on the formulation.

(a) Show that the stress function satisfies the equilibrium equation when the bending stress is computed from

$$\sigma_z = -\frac{P(L-z)y}{I}$$

and $\sigma_x = \sigma_y = \tau_{xy} = 0$. L is the length of the beam.

(b) Develop a weak form for the problem in terms of the stress function ϕ.

(c) For a finite element formulation develop the relation to compute the boundary condition for the case when either three-node triangular or four-node rectangular elements are used.

(d) Write a program to determine the boundary values for the cross-section shown in Fig. 5.21b. Let $w = 2$ and $h = 3$. Use the quasi-harmonic thermal element in *FEAPpv* (or any other available program) to solve for the stress function ϕ. Plot the distribution for ϕ on the cross-section.

(e) Modify the expressions in *FEAPpv* (or any other program for which source code is available) to compute the stress distribution on the cross-section. Solve and plot their distribution. Compare your results to those computed from the classical strength of materials approach.

Hint: Normalize your solution by the factor $P/2I$ to simplify expressions.

5.9 A long sheet pile is placed in soil as shown in Fig. 5.22. The anisotropic properties of the soil are oriented so that $x = x'$ and $y = y'$. The governing differential equation is given in Section 5.3.3. The soil has the properties $k_x = 2$ and $k_y = 3$. Use *FEAPpv* (or any other available program) to determine the distribution of

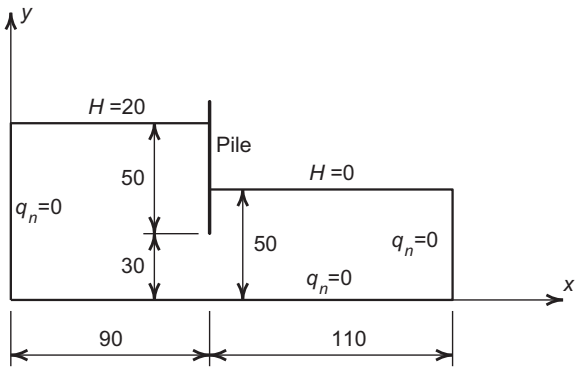

FIGURE 5.22
Seepage under a sheet pile for Problem 5.9.

head and the flow in the region shown. Solve the problem using a mesh of four-node, eight-node, and nine-node quadrilateral elements. Model the problem so that there are about four times as many four-node elements as used for the eight- and nine-node models (and thus approximately an equal number of nodes for each model). Compare total flow obtained from each analysis.

5.10 An axisymmetric sheet pile is placed in soil as shown in Fig. 5.23. The anisotropic properties of the soil are oriented so that $r = r'$ and $z = z'$. The governing equation for plane flow is given in Section 5.3.3. Deduce the Euler differential equation for the axisymmetric problem from the weak form and definitions given in Section 5.1.2.1 suitably modified for the seepage problem.

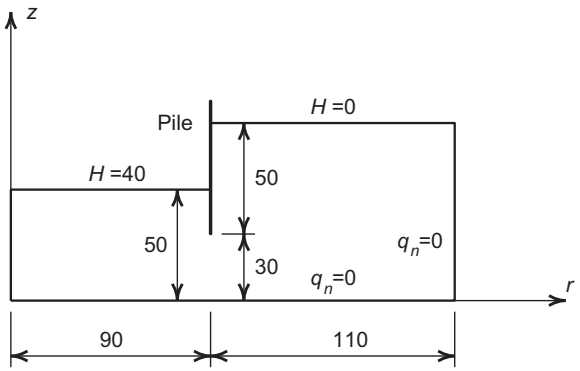

FIGURE 5.23
Seepage under an axisymmetric sheet pile for Problem 5.10.

Assuming isotropic properties with $k = 3$, use *FEAPpv* (or any other available program) to determine the distribution of head and the flow in the region shown. Solve the problem using a mesh of four-node, eight-node, and nine-node quadrilateral elements. Model the problem so that there are about four times as many four-node elements as used for the eight- and nine-node models (and thus approximately an equal number of nodes for each model). Compare total flow obtained from each analysis.

5.11 A membrane occupies a region in the x-y plane and is stretched by a uniform tension T. When subjected to a transient load $q(x, y, t)$ acting normal to the surface the governing differential equation is given by

$$-T\left[\frac{\partial^2 u}{\partial x^2} + \frac{\partial^2 u}{\partial y^2}\right] + m\frac{\partial^2 u}{\partial t^2} = q(x, y, t)$$

(a) Construct a weak form for the differential equation for the case when boundary conditions are given by $u(s, t) = 0$ for s on Γ.

(b) Show that the solution by a finite element method may be constructed using C_0 functions.

(c) Approximate the u and δu by C_0 shape functions $N_a(x, y)$ and determine the semi-discrete form of the equations.

(d) For the case of steady harmonic motion, u may be replaced by

$$u(x, y, t) = w(x, y) \exp i\omega t$$

where $i = \sqrt{-1}$ and ω is the frequency of excitation.
Using this approximation, deduce the governing equation for w. Construct a weak form for this equation. Using C_0 approximations for w determine the form of the discretized problem.

5.12 Program development project:[2] Write a MATLAB [47] or GNU Octave [48] program[3] to solve plane and axisymmetric quasi-harmonic problems.
Your program system should have the following features:

(a) Input module which describes:

(i) Nodal coordinate values, $\mathbf{x}_a$

(ii) Nodes connected to each element and material properties of the element

(iii) Node and degree-of-freedom (dof) for each applied nodal flux force (for problems in this chapter only one degree of freedom is used, however later we will use more)

[2] If programming is included as a part of your study, it is recommended that this problem be solved. Several extensions will be suggested later to create a solution system capable of performing additional steps of finite element analysis.

[3] Another programming language may be used, however, MATLAB and GNU Octave offer many advantages to write simple programs and are also useful to easily complete later exercises.

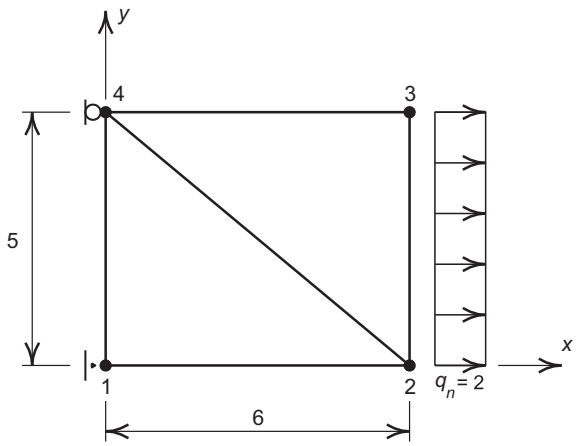

FIGURE 5.24
Patch test for triangles for Problem 5.12.

(iv) Node and dof for fixed (essential) boundary condition—also value if nonzero.

(b) Module to compute the **H** matrix for a three-node triangular element
(c) Module to assemble element arrays into global arrays and specified nodal forces and displacements
(d) Module to solve $\mathbf{H}\tilde{\boldsymbol{\phi}} = \mathbf{s}$
(e) Module to output nodal and element values.

Use your program to solve the *patch test* problem shown in Fig. 5.24. Use the properties $k = 200$ and $q_n = 1$. You can verify the correctness of your answer by computing an exact solution to the problem. The correctness of computed arrays may be obtained using results from *FEAPpv* (or any available quasi-harmonic program).

5.13 Program development project: Add a graphics capability to the program developed in Problem 5.12 to plot contours of the computed finite element ϕ. (Hint: MATLAB has `contour` and `surf` options to easily perform this operation.) Solve a two-dimensional plane problem of your choice and plot contours for ϕ.

5.14 Program development project: Extend the program developed in Problem 5.12 to solve transient problems.
Include an input module to specify the initial temperatures.
Also add a capability to consider time-dependent source terms for Q.
Test your program by solving the square cross-section problem described in Section 5.3.2.

References

[1] O.C. Zienkiewicz, Y.K. Cheung, Finite elements in the solution of field problems, The Engineer, September 1965, pp. 507–510.

[2] W. Visser, A finite element method for the determination of non-stationary temperature distribution and thermal deformation, in: Proceedings of the First Conference on Matrix Methods in Structural Mechanics, vol. AFFDL-TR-66-80, Wright Patterson Air Force Base, Ohio, October 1966.

[3] O.C. Zienkiewicz, P. Mayer, Y.K. Cheung, Solution of anisotropic seepage problems by finite elements, J. Eng. Mech., ASCE 92 (1) (1966) 111–120.

[4] O.C. Zienkiewicz, P.L. Arlett, A.K. Bahrani, Solution of three-dimensional field problems by the finite element method, The Engineer, October 1967.

[5] L.R. Herrmann, Elastic torsion analysis of irregular shapes, J. Eng. Mech., ASCE 91 (6) (1965) 11–19.

[6] A.M. Winslow, Numerical solution of the quasi-linear Poisson equation in a non-uniform triangle 'mesh', J. Comput. Phys. 1 (1966) 149–172.

[7] S. Govindjee, J. Strain, T.J. Mitchell, R.L. Taylor, Convergence of an efficient local least-squares fitting method for bases with compact support, Comput. Methods Appl. Mech. Eng. 213–216 (2012) 84–92, doi: http://dx.doi.org/10.1016/j.cma.2011.11.017.

[8] R. Courant, Variational methods for the solution of problems of equilibrium and vibration, Bull. Am. Math. Soc. 49 (1943) 1–61.

[9] M.J. Turner, R.W. Clough, H.C. Martin, L.J. Topp, Stiffness and deflection analysis of complex structures, J. Aeronaut. Sci. 23 (1956) 805–823.

[10] D.N. de G. Allen, Relaxation Methods, McGraw-Hill, London, 1955.

[11] J.F. Ely, O.C. Zienkiewicz, Torsion of compound bars—a relaxation solution, Int. J. Mech. Sci. 1 (1960) 356–365.

[12] P. Silvester, M.V.K. Chari, Non-linear magnetic field analysis of DC machines, Trans. IEEE (7) (1970) 5–89.

[13] P. Silvester, M.S. Hsieh, Finite element solution of two dimensional exterior field problems, Proc. IEEE 118 (1971).

[14] B.H. McDonald, A. Wexler, Finite element solution of unbounded field problems, Proc. IEEE MTT-20 (12) (1972).

[15] E. Munro, Computer design of electron lenses by the finite element method, in: Image Processing and Computer Aided Design in Electron Optics, Academic Press, New York, 1973, p. 284.

[16] D.V. Tanesa, I.C. Rao, Student Project Report on Lubrication, Royal Naval College, 1966.

[17] M.M. Reddi, Finite element solution of the incompressible lubrication problem, Trans. Am. Soc. Mech. Eng. 91 (Ser. F) (1969) 524.

[18] M.M. Reddi, T.Y. Chu, Finite element solution of the steady state compressible lubrication problem, Trans. Am. Soc. Mech. Eng. 92 (Ser. F) (1970).

[19] J.H. Argyris, D.W. Scharpf, The incompressible lubrication problem, J. Roy. Aeronaut. Soc. 73 (1969) 1044–1046.
[20] J.F. Booker, K.H. Huebner, Application of finite element methods to lubrication: an engineering approach, J. Lubr. Technol., Trans. ASME 14 (Ser. F) (1972) 313.
[21] K.H. Huebner, Application of finite element methods to thermohydrodynamic lubrication, Int. J. Numer. Methods Eng. 8 (1974) 139–168.
[22] S.M. Rohde, K.P. Oh, Higher order finite element methods for the solution of compressible porous bearing problems, Int. J. Numer. Methods Eng. 9 (1975) 903–912.
[23] A.K. Tieu, Oil film temperature distributions in an infinitely wide glider bearing: an application of the finite element method, J. Mech. Eng. Sci. 15 (1973) 311.
[24] K.H. Huebner, Finite element analysis of fluid film lubrication—a survey, in: R.H. Gallagher, J.T. Oden, C. Taylor, O.C. Zienkiewicz (Eds.), Finite Elements in Fluids, vol. II, John Wiley & Sons, New York, 1975, pp. 225–254.
[25] A. Curnier, R.L. Taylor, A thermomechanical formulation and solution of lubricated contacts between deformable solids, J. Lubr. Technol., ASME 104 (1982) 109–117.
[26] H.C. Martin, Finite element analysis of fluid flows, in: Proceedings of the Second Conference on Matrix Methods in Structural Mechanics, vol. AFFDL-TR-68-150, Wright Patterson Air force Base, Ohio, October 1968.
[27] G. de Vries, D.H. Norrie, Application of the finite element technique to potential flow problems, Technical Report, Reports 7 and 8, Dept. Mech. Eng., University of Calgary, Alberta, Canada, 1969.
[28] J.H. Argyris, G. Mareczek, D.W. Scharpf, Two and three dimensional flow using finite elements, J. Roy. Aeronaut. Soc. 73 (1969) 961–964.
[29] L.J. Doctors, An application of finite element technique to boundary value problems of potential flow, Int. J. Numer. Methods Eng. 2 (1970) 243–252.
[30] G. de Vries, D.H. Norrie, The application of the finite element technique to potential flow problems, J. Appl. Mech., ASME 38 (1971) 798–802.
[31] S.T.K. Chan, B.E. Larock, L.R. Herrmann, Free surface ideal fluid flows by finite elements, J. Hydraul. Div., ASCE 99 (6) (1973).
[32] B.E. Larock, Jets from two dimensional symmetric nozzles of arbitrary shape, J. Fluid Mech. 37 (1969) 479–483.
[33] O.C. Zienkiewicz, R.L. Taylor, P. Nithiarasu, The Finite Element Method for Fluid Dynamics, Elsevier, Oxford, seventh ed., 2013.
[34] C.S. Desai, Finite element methods for flow in porous media, in: J.T. Oden, O.C. Zienkiewicz, R.H. Gallagher, C. Taylor (Eds.), Finite Elements in Fluids, vol. 1, John Wiley & Sons, New York, 1976, pp. 157–182.
[35] I. Javandel, P.A. Witherspoon, Applications of the finite element method to transient flow in porous media, Trans. Soc. Petrol. Eng. 243 (1968) 241–251.
[36] R.L. Taylor, C.B. Brown, Darcy flow solutions with a free surface, J. Hydraul. Div., ASCE 93 (2) (1967) 25–33.

[37] J.C. Luke, A variational principle for a fluid with a free surface, J. Fluid Mech. 27 (1957) 395–397.
[38] K. Washizu, Variational Methods in Elasticity and Plasticity, Pergamon Press, New York, third ed., 1982.
[39] J.C. Bruch, A survey of free-boundary value problems in the theory of fluid flow through porous media, Adv. Water Resour. 3 (1980) 65–80.
[40] C. Baiocchi, V. Comincioli, V. Maione, Unconfined flow through porous media, Meccanice, Ital. Ass. Theor. Appl. Mech. 10 (1975) 51–60.
[41] J.M. Sloss, J.C. Bruch, Free surface seepage problem, J. Eng. Mech., ASCE 108 (5) (1978) 1099–1111.
[42] N. Kikuchi, Seepage flow problems by variational inequalities, Int. J. Numer. Anal. Methods Geomech. 1 (1977) 283–290.
[43] C.S. Desai, Finite element residual schemes for unconfined flow, Int. J. Numer. Methods Eng. 10 (1976) 1415–1418.
[44] C.S. Desai, G.C. Li, A residual flow procedure and application for free surface, and porous media, Adv. Water Resour. 6 (1983) 27–40.
[45] K.J. Bathe, M. Koshgoftar, Finite elements from surface seepage analysis without mesh iteration, Int. J. Numer. Anal. Methods Geomech. 3 (1979) 13–22.
[46] S.P. Timoshenko, J.N. Goodier, Theory of Elasticity, McGraw-Hill, New York, second ed., 1951.
[47] MATLAB, 2012. <www.mathworks.com>.
[48] GNU Octave, 2012. <www.gnu.org/software/octave>.
[49] O.C. Zienkiewicz, R.L Taylor, J.Z. Zhu, The Finite Element Method: Its Basis & Fundamentals, Elsevier, Oxford, sixth ed., 2005.